Publication VII

Sami Ilvonen and Ilkka Laakso. 2009. Computational estimation of magnetically induced electric fields in a rotating head. Physics in Medicine and Biology, volume 54, number 2, pages 341-351.

IOP PUBLISHING PHYSICS IN MEDICINE AND BIOLOGY

Phys. Med. Biol. **54** (2009) 341–351 doi:10.1088/0031-9155/54/2/011

Computational estimation of magnetically induced electric fields in a rotating head

Sami Ilvonen and Ilkka Laakso

Department of Radio Science and Engineering, Helsinki University of Technology, Otakaari 5 A, 02150 Espoo, Finland

E-mail: sami.ilvonen@tkk.fi

Received 11 September 2008, in final form 24 October 2008
Published 19 December 2008
Online at stacks.iop.org/PMB/54/341

Abstract

Change in a magnetic field, or similarly, movement in a strong static magnetic field induces electric fields in human tissues, which could potentially cause harmful effects. In this paper, the fields induced by different rotational movements of a head in a strong homogeneous magnetic field are computed numerically. Average field magnitudes near the retinas and inner ears are studied in order to gain insight into the causes of phosphenes and vertigo-like effects, which are associated with extremely low-frequency (ELF) magnetic fields. The induced electric fields are calculated in four different anatomically realistic head models using an efficient finite-element method (FEM) solver. The results are compared with basic restriction limits by IEEE and ICNIRP. Under rotational movement of the head, with a magnetic flux rate of change of 1 T s^{-1}, the maximum IEEE-averaged electric field and maximum ICNIRP-averaged current density were 337 mV m^{-1} and 8.84 mA m^{-2}, respectively. The limits by IEEE seem significantly stricter than those by ICNIRP. The results show that a magnetic flux rate of change of 1 T s^{-1} may induce electric field in the range of 50 mV m^{-1} near retinas, and possibly even larger values near the inner ears. These results provide information for approximating the threshold electric field values of phosphenes and vertigo-like effects.

(Some figures in this article are in colour only in the electronic version)

1. Introduction

A changing magnetic field, or similarly, movement in a static magnetic field, induces an electric field inside a human body. As these magnetic-field-induced electric fields and currents could potentially cause harmful effects, several bodies have issued regulatory standards and guidelines, such as Institute of Electrical and Electronics Engineers (IEEE 2002), International Commission on Non-Ionizing Radiation Protection (ICNIRP 1998, 2003) and Australian

Radiation Protection and Nuclear Safety Agency (ARPANSA) (Wood 2008). Also the European Union has issued a work safety directive 2004/40/EC, which is largely based on the ICNIRP guidelines.

The induced field may interact with the body by several mechanisms, which include magnetohydrodynamic forces, and sensory or nerve stimulation. The magnitudes of the induced currents are small, so resistive heating (as in the RF frequencies) is negligible. Currently, there are no confirmed long-term biological hazards, and effects are limited to short-term reactions. These short-term sensory effects include magnetic-field-induced vertigo (MFIV), which is associated with head movement in a static magnetic field. It has been proposed in Glover *et al* (2007) that the mechanism behind the vertigo-like effects is the induced galvanic vestibular stimulation (iGVS) by induced electric currents in the vestibular system. In the same study, severe nausea caused by MFIV was reported for some subjects. Also, disorientation due to MFIV might cause indirect injury. Another short-term sensory effect of extremely low-frequency magnetic field is phosphenes, i.e. seeing light flashes. It is likely to be caused by stimulation due to induced electric fields in the retina, and is considered to have the lowest perception threshold for direct sensory effects. The smallest threshold occurs at around 20 Hz, and the threshold rises steeply above 60 Hz, so phosphenes are not important for the higher frequency fields, such as the kHz-range MRI gradient fields. Currently, there is no evidence of the harmfulness of phosphenes. One motivation of this paper is to estimate the magnitudes of the induced electric fields near retina and vestibular system to gain better understanding of these two effects.

The induced currents due to extremely low-frequency magnetic fields have been simulated several times in the literature using different numerical methods. Most popular choices have so far been finite-difference methods, such as the scalar-potential finite-difference method (SPFD) (Dawson *et al* 1996, Dimbylow 1998) and the impedance method (Deford and Gandhi 1985, Orcutt and Gandhi 1988). Also, quasi-static finite-difference time-domain (Potter *et al* 2000), the finite-integration technique and the finite-element method have been used.

Currents induced by power frequency and above magnetic and electric fields have been studied *inter alia* in Dawson *et al* (1998), where whole-body exposure to 60 Hz magnetic field was simulated; Dimbylow (1998) for exposure to 50 Hz–10 MHz magnetic field; Caputa *et al* (2002), where, e.g., the effects of resolution and model variation were studied and Dimbylow (2008), which studied male and female models exposed to 50 Hz magnetic and electric fields, and compared different field-averaging methods. Compared to these studies, the present case has mostly the same underlying equations, only with different source terms.

Similar numerical methods have been applied for the safety assessment of magnetic fields of magnetic resonance imaging (MRI) scanners in several studies. Induced electric fields by kHz-range magnetic field gradient coils have been simulated for various human models by Liu *et al* (2003b), Mao *et al* (2006), Bencsik *et al* (2007) and Crozier *et al* (2007). Finally, movement-induced electric fields in spatially inhomogeneous static magnetic fields of a MR scanner have been studied by Liu *et al* (2003a) and Crozier and Liu (2005). Glover *et al* (2007) recently performed measurements with volunteers and studied the effects of movement in a static magnetic field under various exposure conditions. In another study by Glover and Bowtell (2008), the induced surface electric fields were measured during natural body movements in the magnetic field of the MRI scanner.

The goal of this paper is to produce information for approximating the threshold electric field values of phosphenes and MFIV effects associated with movements of the head in a static magnetic field. Computed results are also compared to the basic restriction limits set by IEEE and ICNIRP in order to estimate the compliance of different rotational head movements in a

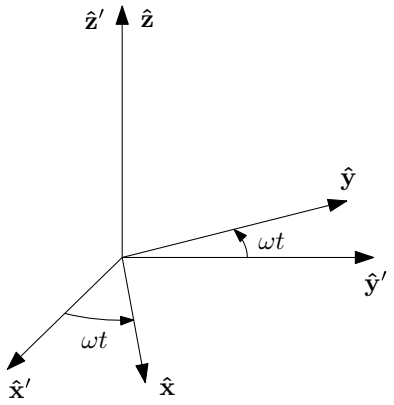

Figure 1. Rotating coordinate frames. Primed vectors denote the static reference coordinate system Γ'. The coordinate system Γ of the body is rotating with an angular velocity of ω with respect to the reference system.

strong static magnetic field, e.g. near MRI scanners. For these purposes, the induced electric field is solved using the finite-element method (FEM). Various rotational movements for four different head models are studied.

2. Methods

2.1. Theory

Let us consider a case with a constant, homogeneous source magnetic flux density $\mathbf{B}_0'(\mathbf{r}') = B_0\hat{\mathbf{x}}'$ in the reference coordinate system Γ' with a position vector $\mathbf{r}' = x'\hat{\mathbf{x}}' + y'\hat{\mathbf{y}}' + z'\hat{\mathbf{z}}'$ shown in figure 1. If a rigid conducting body rotating with a constant angular velocity ω around the z'-axis is placed in this static magnetic field, the source magnetic flux density in the coordinate system Γ of the object is $\mathbf{B}_0(\mathbf{r}, t) = B_0(\hat{\mathbf{x}}\cos\omega t - \hat{\mathbf{y}}\sin\omega t)$. The time derivative of this field is

$$\frac{\partial}{\partial t}\mathbf{B}_0(\mathbf{r}, t) = -\omega B_0(\hat{\mathbf{x}}\sin\omega t + \hat{\mathbf{y}}\cos\omega t). \tag{1}$$

This changing (in the frame Γ) magnetic flux density induces currents into the rotating object.

Since we want to solve the induced electric field and currents using the well known and efficient quasi-static scalar potential formulation, see, e.g. Dawson *et al* (1996) or Liu *et al* (2003b), we have to express the source magnetic flux density in terms of a vector potential $\mathbf{A}_0(\mathbf{r}, t)$ fulfilling the condition $\mathbf{B}_0(\mathbf{r}, t) = \nabla \times \mathbf{A}_0(\mathbf{r}, t)$. Simple manipulation shows that we can choose

$$\frac{\partial}{\partial t}\mathbf{A}_0(\mathbf{r}, t) = \hat{\mathbf{z}}\omega B_0(x\cos\omega t - y\sin\omega t), \tag{2}$$

which is equal to the Lorentz force term $\mathbf{v} \times \mathbf{B}$ for this case. Ignoring self-induction, the induced electric field can now be expressed as

$$\mathbf{E}(\mathbf{r}, t) = -\nabla\phi(\mathbf{r}, t) - \frac{\partial}{\partial t}\mathbf{A}_0(\mathbf{r}, t). \tag{3}$$

Under quasi-static approximation, $\nabla \cdot \sigma \mathbf{E} = 0$, and the unknown scalar potential $\phi(\mathbf{r}, t)$ can be solved from equation

$$\nabla \cdot (\sigma(\mathbf{r}) \nabla \phi(\mathbf{r}, t)) = -\nabla \cdot \left(\sigma(\mathbf{r}) \frac{\partial}{\partial t} \mathbf{A}_0(\mathbf{r}, t) \right), \tag{4}$$

where $\sigma(\mathbf{r})$ denotes the conductivity of the moving body. The boundary condition on the outer boundary is $\hat{\mathbf{n}} \cdot \sigma \mathbf{E} = 0$, where $\hat{\mathbf{n}}$ is the normal vector.

From equation (1), one can see that it suffices to solve two cases, $\omega t = 0$ and $\omega t = \pi/2$, in order to construct the solution for any angle ωt. Furthermore, solution for each fixed t is identical to a problem where the object is stationary, and the source is a homogeneous $\frac{\partial}{\partial t}\mathbf{B}_0$ field with $\left|\frac{\partial}{\partial t}\mathbf{B}_0\right| = \omega B_0$, and the direction is determined by t. It is also worth noticing that the source magnetic flux density parallel to the direction of the rotation axis does not induce any currents. Instead, it generates a rotation-induced potential, which is static when the rotation speed is constant.

2.2. *Computational method*

The unknown scalar potential ϕ in equation (4) was solved using the finite-element method (FEM). The solver was written using C++ programming language and uses components from an open source software suite Trilinos (Heroux *et al* 2005), which includes the needed data structures for sparse matrix computations and a wide variety of solvers for matrix equations. Correctness of the solver was validated by comparing the computed results of several model problems with the results obtained using a commercial FEM solver (Comsol Multiphysics, Comsol AB, Sweden).

Since the generation of tetrahedral meshes was not feasible for the whole head models with all tissues, we used simple cubical meshes in all simulations. In this approach, each material voxel corresponds to a cubical trilinear FEM element with an unknown node value on each corner of the cube. The uniform cubical mesh allowed efficient calculation of the matrix–vector product without the need to assemble the whole system matrix, which lead to significant memory savings. After the unknown potential had been solved, the induced electric field was computed using equation (3).

Since the resulting matrix equation is symmetric and positive definite, we used the conjugate gradient (CG) method. The CG solver was preconditioned with ML (Gee *et al* 2006), which is an algebraic multigrid (AMG) preconditioner and part of the Trilinos suite. In all cases, the iteration was continued until the relative residual norm was below 10^{-10}, which required roughly 15 iterations. The longest solution time for a model with about five million unknowns was 5 min using an ordinary desktop PC with 4 GB of memory.

2.3. *ICNIRP and IEEE averaging methods*

The ICNIRP guideline requires that the computed current density is averaged over a 1 cm^2 area perpendicular to the direction of the current. This approach has been somewhat problematic, as recently discussed by Dimbylow (2008). Also the role of the induced current as the basic restriction criteria has been questioned and the induced electric field is considered to be a more reliable quantity (Wood 2008).

In this work, we estimated the compliance using both the ICNIRP guideline (ICNIRP 1998) and the IEEE standard C95.6 (IEEE 2002). The ICNIRP averaging of the currents induced in the central nervous system (CNS) was computed as in Ilvonen and Sarvas (2007) using three perpendicular circular masks. Only the values belonging to the CNS were considered. A worst-case approximation was then determined from these three averaged

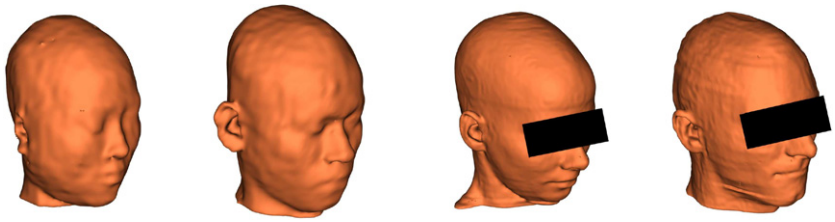

Figure 2. Head models from left to right: Japanese female, Japanese male, European female (Ella) and European male (Duke).

current components as $J_{\text{avg}} = \max\left(\sqrt{J_x^2 + J_y^2 + J_z^2}\right)$. For the IEEE compliance evaluation, each Cartesian component of the induced electric field inside the CNS was averaged over a 5 mm distance in a direction parallel to the component. The worst-case approximation was then computed similarly to the ICNIRP averaging. For 2 mm models, the averages were computed as a weighted sum, so that the effective distance in the Cartesian mesh was 5 mm.

3. Models

3.1. Head models

Four head models were used in this study. The first two models were Japanese 22 year old male and female voxel models constructed from MRI data (Nagaoka *et al* 2004), both having a spatial resolution of 2 mm. The other two models were European 34 year old male (Duke) and 26 year old female (Ella) CAD models constructed from MR images, originating from the Virtual family (VF) project (Christ *et al* 2008). The CAD models were used to produce 2 mm and 1 mm resolution voxel data. Originally, all four models were whole-body models, but for this study, only the heads were used. The head models are shown in figure 2. Conductivity values for different tissues were those in Gabriel *et al* (1996a, 1996b, 1996c), calculated for 10 Hz frequency. This frequency is obviously higher than the frequencies involved in natural head movements, but it serves as the best-available estimate.

3.2. Inner ear averaging

Information about electric field distribution in the inner ear could be useful for the assessment of vertigo and iGVS. Unfortunately, none of the four head models includes inner ear or vestibular system. Additionally, in the Japanese models, the bone surrounding the inner ear is modelled as air, which makes even crude estimation of electric field unreasonable. In the VF head models, the same region is modelled as bone, which at least allows some rough approximation of typical field magnitudes. As the VF models do not contain inner ear model, the induced electric field was averaged over two 1 cm^3 cubical volumes chosen from the vicinities of each of the inner ears as

$$E_{\text{avg}} = \sqrt{\frac{1}{N}\sum_{i=1}^{N} |\mathbf{E}_i|^2}, \tag{5}$$

where $\mathbf{E}_i$ are the electric field values in each element, and N is the number of values in the averaging volume.

Table 1. Tissue composition in the back of the eye near retina.

Tissue	Japanese male	Japanese female	Duke	Ella
Eye tissue[a]	48.7%	48.8%	49.1%	49.3%
Fat	45.8%	48.6%	43.4%	26.6%
Muscle	4.5%	2.6%	3.0%	19.3%
Other[b]	1.0%	0.0%	4.4%	4.8%

[a] Includes vitreous humour and sclera.
[b] Includes connective tissue and nerve.

3.3. Retina averaging

Induced electric field in the retina may cause phosphenes generation. In Lövsund *et al* (1980a, 1980b), the most sensitive frequency for phosphenes generation is found to be 20 Hz. While the models are coarse, calculating typical magnitudes of induced field near the retina is possible. As the spatial resolution of the models is in the range of 1–2 mm, the models do not contain retina models. In the Japanese models, the eye consists of only three tissues: vitreous humour, lens and cornea, where the vitreous humour also includes sclera. In addition to the above three tissues, the VF models include a separate sclera model, which is 2 mm thick. In this work, this too large thickness was taken into account by setting the conductivity of the sclera tissue to the average of sclera and vitreous humour. For all models, the conductivity of fat—including the orbital fat—was chosen to be that of 'not infiltrated fat' in Gabriel *et al* (1996c).

The approximate electric field near the retina was calculated over a 4 mm (two or four cells) thick layer at the back of the eye using equation (5). Volume of the layer is approximately 2 cm^3 ($\pm 10\%$), which is sufficient for smoothing out possible large point-wise peak values due to inherent geometrical artefacts. The detailed tissue composition of the layer is presented in table 1. There are no significant differences between left and right eyes of the same model. The tissue compositions of the models are generally quite similar, but the VF female model has significantly more muscle tissue behind the eye than the other models.

3.4. Rotation patterns

The head movement was studied for three different rotation axes, which are illustrated in figure 3. The directions of the rotation axes were determined manually. Naturally, the axes are only suggestive, as realistic head movements involve the joints between the cervical vertebrae and the atlanto-occipital joint. Only bulk movement of the head was considered, i.e. the electric field induced by internal movement, such as blood flow, was ignored. Full rotations of 360° were computed, so that the maximum value of induced electric field could be determined for any incoming magnetic field direction.

4. Results

In the presented results, the amplitude of the magnetic flux density is constant (1 T) and the angular velocity of the head movement is 1 s^{-1}. Thus, the amplitude of the rate of change of the magnetic flux density is uniform (1 T s^{-1}) throughout the entire head. The induced electric field depends linearly on the rate of change of the magnetic flux density, so simple multiplication gives the results for any other value of $\mathrm{d}B_0/\mathrm{d}t$. As measured by Glover and Bowtell (2008), natural movement in the fringe fields of the MRI scanner may typically have $\mathrm{d}B_0/\mathrm{d}t$ values as high as 3 T s^{-1} (3 T magnet).

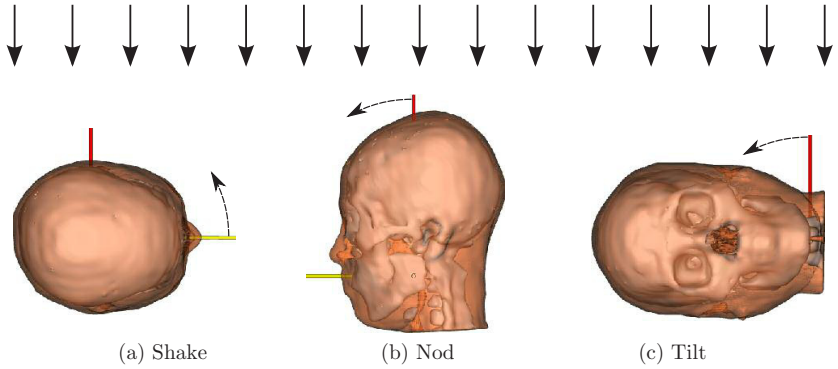

Figure 3. Three rotational head movements: cervical rotation (shake), cervical flexion (nod) and cervical lateral flexion (tilt). Arrows on the top show the direction of incoming magnetic field. Three smaller arrows show the rotation direction of the head. Rotation angles in the figure are 0°, with external magnetic field pointing downwards.

The rotation angles, which tell the direction of the head with respect to the external magnetic field, are shown in figure 3. As the presented results are norms and absolute values, they are modulo 180°. Naturally, rotational movement is analogous to the case where the direction of the external magnetic field is rotating. Also, each rotation angle corresponds to a case where the head is stationary and the source is a constant homogeneous $\mathrm{d}\mathbf{B}_0/\mathrm{d}t$ field, as explained in section 2.1. The direction of $\mathrm{d}\mathbf{B}_0/\mathrm{d}t$ is orthogonal to the external magnetic field. Thus, for example, the results for an applied $\mathrm{d}B_0/\mathrm{d}t$ in the up–down direction are the same as the results for nodding motion at 90° or tilting motion at 0°.

Table 2 shows the averages of the induced electric field over the region near the retinas and inner ears as described in sections 3.2 and 3.3. In the table, the results were simulated with conductivity values calculated at 10 Hz. When using the conductivity values of 20 Hz, which might be the most sensitive frequency to phosphenes, the resulting induced electric field was generally slightly smaller. In the retinas, this difference in average electric field was 2.9 mV m^{-1} at the maximum, resulting in the relative difference of approximately 7%. This is well within the limits of modelling uncertainty, and the presented results can also be used for 20 Hz, in which case the results should be interpreted for the applied magnetic field, because rotation speeds such as this are obviously beyond the limits of any normal human being.

The variation of the average electric field was somewhat sinusoidal with the rotation angle. The rotation angle which gives the minimum electric field is approximately the maximum angle shifted by 90°. It seems that the rotation angles which give the maximum and minimum fields approximately match the maximum and minimum values of local $\mathbf{v} \times \mathbf{B}_0$. For example, shaking motion gives the maximum electric field in the left retina at 61°–75°, which in figure 3 corresponds to the instant when the local velocity in the left eye is orthogonal to the external magnetic field.

To compare our results with the measurements by Glover and Bowtell (2008), averaged induced electric field on a 4 mm thick layer on the top of the tongue was calculated, using equation (5). For the nodding motion, the maximum average electric field was reached when the magnetic field direction was away from (or towards) the face. The average maximum value with standard deviation was 14 ± 2 mV m^{-1}, and the minimum value was 4.8 ± 1.0 mV m^{-1}, the magnetic field direction being vertical. Shaking motion gave the maximum value 18 ± 5 mV m^{-1} and the minimum value 6.7 ± 0.9 mV m^{-1}, at rotation angles 90° and

Table 2. Averaged electric field near retinas and inner ears for the three studied rotation patterns. The electric field values are in mV m^{-1}. Max and min columns show the maximum and minimum values during one full rotation. Angle column shows the rotation angle (figure 3) which gives the maximum electric field.

	Shake			Nod			Tilt		
Left retina	Max	Angle	Min	Max	Angle	Min	Max	Angle	Min
Left retina									
Japanese female	37.2	68°	6.3	33.2	−80°	14.6	36.1	−55°	31.6
Japanese male	49.4	68°	8.8	29.6	76°	19.9	47.5	−85°	29.0
Ella 2 mm	47.9	76°	7.1	29.4	−65°	9.9	50.9	−63°	10.7
Ella 1 mm	54.4	75°	7.5	30.3	−62°	11.4	55.8	−67°	12.7
Duke 2 mm	44.4	62°	5.3	26.1	−85°	19.3	39.8	−77°	24.7
Duke 1 mm	68.1	63°	6.5	38.0	−84°	28.6	60.9	−81°	36.5
Right retina									
Japanese female	37.1	−72°	5.9	39.5	−85°	11.8	39.5	9°	35.2
Japanese male	46.4	−68°	9.8	39.9	90°	19.2	46.7	47°	32.7
Ella 2 mm	44.9	−73°	7.0	28.5	−67°	9.9	49.2	62°	11.5
Ella 1 mm	51.5	−72°	7.3	29.7	−64°	11.4	54.5	65°	13.6
Duke 2 mm	36.6	−66°	5.1	26.4	−87°	15.4	35.7	64°	23.3
Duke 1 mm	54.3	−67°	6.3	34.9	−79°	20.3	53.0	68°	29.2
L inner ear									
Ella 2 mm	64.4	3°	8.1	73.1	−30°	29.1	38.7	4°	7.7
Ella 1 mm	66.0	1°	9.6	73.3	−27°	29.6	37.4	7°	9.1
Duke 2 mm	113.1	2°	14.0	113.2	−17°	56.6	59.2	−11°	9.5
Duke 1 mm	115.6	2°	13.3	115.5	−16°	52.2	54.7	−11°	9.0
R inner ear									
Ella 2 mm	60.8	−4°	8.7	65.0	−24°	34.3	37.8	1°	11.6
Ella 1 mm	62.8	−3°	10.8	66.1	−20°	31.3	33.8	2°	12.7
Duke 2 mm	124.0	−4°	10.6	124.5	−7°	50.9	51.3	5°	12.7
Duke 1 mm	131.1	−3°	10.4	131.7	−7°	48.7	49.1	4°	12.8

Table 3. Maximum values obtained using ICNIRP and IEEE averaging methods for different rotation patterns.

	Shake		Nod		Tilt	
Model	IEEE (mV m^{-1})	ICNIRP (mA m^{-2})	IEEE (mV m^{-1})	ICNIRP (mA m^{-2})	IEEE (mV m^{-1})	ICNIRP (mA m^{-2})
Japanese female	240	5.13	183	4.02	181	5.13
Japanese male	209	8.05	186	4.48	182	8.01
Ella 2 mm	235	6.56	225	4.14	236	6.57
Ella 1 mm	294	6.51	202	3.73	294	6.52
Duke 2 mm	288	7.07	196	3.74	288	7.07
Duke 1 mm	337	8.83	200	3.63	337	8.84

0°, respectively. Table 3 shows the spatial maxima of IEEE- and ICNIRP-averaged electric fields as described in section 2.3. The presented values are maximum values over all rotation angles, for each rotation pattern separately. The mean values over all rotation angles were just 10–35% smaller than the maximum values.

5. Discussion

It has been suggested in Glover and Bowtell (2008) that induced electric field could be related to the external magnetic field by a location-specific geometry factor, i.e. the ratio between the induced electric field and the rate of change of the magnetic flux density. In that study, the left–right component of the electric field on top of the tongue was measured, and the resulting geometry factor was derived to be 15 ± 2 mm. Our simulated results for the top of the tongue match this well, giving the maximum geometry factors 14 ± 2 mm and 18 ± 5 mm, for nodding and shaking motions, respectively. While the simulated geometry factors are certainly similar in magnitude with the measured results, there could be large variations depending on the direction of the time derivative of the magnetic field. For the rotation angles which give the maximum electric fields, the mean geometry factors (with standard deviation) of the retina are 48 ± 9 mm for shaking, 32 ± 5 mm for nodding and 47 ± 8 mm for tilting motion. For the vicinity of the inner ears, the corresponding geometry factors are 92 ± 31 mm, 95 ± 28 mm and 45 ± 9 mm. The directions which gave the maximum local induced electric field seemed to approximately match the maximum directions of local $|\mathbf{v} \times \mathbf{B}_0|$.

Maximum values for IEEE- and ICNIRP-averaged electric field and current were 337 mV m^{-1} and 8.84 mA m^{-2}, respectively. Neither IEEE nor ICNIRP have specified how the basic restriction limits should be applied for movement-induced fields, so we have used the approach for non-sinusoidal waveforms and multiplied the rms basic restriction limits by $\sqrt{2}$. Consequently, to ensure that IEEE limits for occupational exposure are not exceeded, the rate of change of the magnetic flux density should be limited to 0.074 T s^{-1}, assuming that the frequencies are below 20 Hz. For ICNIRP, the values should be limited to 6.4 T s^{-1} up to 1 Hz and 1.6 T s^{-1} above 4 Hz. According to Glover *et al* (2007), phosphenes were routinely perceived during measurements for values of 1.5 T s^{-1} (50 ms pulsed magnetic field). Vertigo was reported for field changes larger than 2 T and time derivative exceeding 1.5 T s^{-1} for times greater than 1 s (head movement), causing even severe nausea for some subjects. It seems that the basic restriction limits by ICNIRP might be non-conservative when it comes to preventing phosphenes or MFIV. On the other hand, even slow rotational motion near the MRI scanner is likely to cause the IEEE limits to be exceeded. Direct comparison of IEEE and ICNIRP limits is, however, difficult due to the frequency dependency and uncertainties of the conductivity values at frequencies below 10 Hz.

In a recent literature analysis by Wood (2008), the threshold for phosphenes occurrence is approximated as a 'power of ten' value of 100 mV m^{-1} at 20 Hz, although with a large range of uncertainty. In IEEE standard (IEEE 2002), this limit has been derived to be 75 mV m^{-1}. If our results are used for 20 Hz magnetic field, these thresholds could be exceeded for magnetic flux time derivative values of 1.6–2.1 T s^{-1}, for the worst-case magnetic field direction. For vertical $\mathrm{d}B_0/\mathrm{d}t$, which was used in, e.g., Glover *et al* (2007), these thresholds might be exceeded for 2.3–3.1 T s^{-1}, which suggests that the threshold may actually be somewhat lower.

6. Conclusions

An effective finite-element method solver has been used to simulate electric fields induced in the head by extremely low-frequency magnetic fields. Especially, the fields induced by the rotational movement of the head in a homogeneous static magnetic field have been investigated for four anatomically realistic head models. Average induced electric field near retinas and inner ears were calculated. The results could be useful for the safety assessment of static magnetic fields, or for the approximation of the threshold limits for phosphenes generation.

The field averages as required by ICNIRP and IEEE have been calculated, and the results have been compared to basic restriction limits. From the results, it seems that the limits by IEEE are significantly more restrictive than those by ICNIRP, and could be easily exceeded for head movements near the magnetic field of the MRI scanner.

Acknowledgments

Financial support received from GETA (Graduate School in Electronics, Telecommunication and Automation) is acknowledged. Authors also wish to thank Professor Kari Jokela for helpful comments.

References

Bencsik M, Bowtell R and Bowley R 2007 Electric fields induced in the human body by time-varying magnetic field gradients in MRI: numerical calculations and correlation analysis *Phys. Med. Biol.* **52** 2337–53

Caputa K, Dimbylow P J, Dawson T W and Stuchly M A 2002 Modelling fields induced in humans by 50/60 Hz magnetic fields: reliability of the results and effects of model variations *Phys. Med. Biol.* **47** 1391–8

Christ A *et al* 2008 The Virtual Family—development of anatomical CAD models of two adults and two children for dosimetric simulations (in preparation)

Crozier S and Liu F 2005 Numerical evaluation of the fields induced by body motion in or near high-field MRI scanners *Prog. Biophys. Mol. Biol.* **87** 267–78

Crozier S, Wang H, Trakic A and Liu F 2007 Exposure of workers to pulsed gradients in MRI *J. Magn. Reson. Imaging* **26** 1236–54

Dawson T, Caputa K and Stuchly M 1998 High-resolution organ dosimetry for human exposure to low-frequency electric fields *IEEE Trans. Power Deliv.* **13** 366–73

Dawson T W, Moerloose J D and Stuchly M A 1996 Comparison of magnetically induced ELF fields in humans computed by FDTD and scalar potential FD codes *Appl. Comput. Electromagn. Soc. J.* **11** 63–71

Deford J and Gandhi O 1985 An impedance method to calculate currents induced in biological bodies exposed to quasi-static electromagnetic fields *IEEE Trans. Electromagn. Compat.* **EMC-27** 168–73

Dimbylow P 2008 Quandaries in the application of the ICNIRP low frequency basic restriction on current density *Phys. Med. Biol.* **53** 133–45

Dimbylow P J 1998 Induced current densities from low-frequency magnetic fields in a 2 mm resolution, anatomically realistic model of the body *Phys. Med. Biol.* **43** 221–30

Gabriel C, Gabriel S and Corthout E 1996a The dielectric properties of biological tissues: I. Literature survey *Phys. Med. Biol.* **41** 2231–49

Gabriel S, Lau R W and Gabriel C 1996b The dielectric properties of biological tissues: II. Measurements in the frequency range 10 Hz to 20 GHz *Phys. Med. Biol.* **41** 2251–69

Gabriel S, Lau R W and Gabriel C 1996c The dielectric properties of biological tissues: III. Parametric models for the dielectric spectrum of tissues *Phys. Med. Biol.* **41** 2271–93

Gee M, Siefert C, Hu J, Tuminaro R and Sala M 2006 ML 5.0 Smoothed Aggregation User's Guide SAND2006-2649 *Sandia National Laboratories* (Albuquerque, New Mexico, USA)

Glover P M and Bowtell R 2008 Measurement of electric fields induced in a human subject due to natural movements in static magnetic fields or exposure to alternating magnetic field gradients *Phys. Med. Biol.* **53** 361–73

Glover P, Cavin I, Qian W, Bowtell R and Gowland P 2007 Magnetic-field-induced vertigo: a theoretical and experimental investigation *Bioelectromagnetics* **28** 349–61

Heroux M A *et al* 2005 An overview of the Trilinos project *ACM Trans. Math. Softw.* **31** 397–423

ICNIRP 1998 Guidelines for limiting exposure to time-varying electric, magnetic and electromagnetic fields (up to 300 GHz) *Health Phys.* **74** 492–522

ICNIRP 2003 Guidance on determining compliance of exposure to pulsed fields and complex non-sinusoidal waveforms below 100 kHz with ICNIRP guidelines *Health Phys.* **84** 383–7

IEEE 2002 *IEEE Standard for Safety Levels with Respect to Human Exposure to Electromagnetic Fields, 0–3 kHz, IEEE Standard C95.6-2002* (New York: IEEE)

Ilvonen S and Sarvas J 2007 Magnetic-field-induced ELF currents in a human body by the use of a GSM phone *IEEE Trans. Electromagn. Compat.* **49** 294–301

Liu F, Zhao H and Crozier S 2003a Calculation of electric fields induced by body and head motion in high-field MRI *J. Magn. Reson.* **161** 99–107

Liu F, Zhao H and Crozier S 2003b On the induced electric field gradients in the human body for magnetic stimulation by gradient coils in MRI *IEEE Trans. Biomed. Eng.* **50** 804–15

Lövsund P, Öberg P Å and Nilsson S E G 1980a Magneto- and electrophosphenes: a comparative study *Med. Biol. Eng. Comput.* **18** 758–64

Lövsund P, Öberg P Å, Nilsson S E G and Reuter T 1980b Magnetophosphenes: a quantitative analysis of thresholds *Med. Biol. Eng. Comput.* **18** 326–34

Mao W, Chronik B A, Feldman R E, Smith M B and Collins C M 2006 Consideration of magnetically-induced and conservative electric fields within a loaded gradient coil *Magn. Reson. Med.* **55** 1424–32

Nagaoka T, Watanabe S, Sakurai K, Kunieda E, Watanabe S, Taki M and Yamanaka Y 2004 Development of realistic high-resolution whole-body voxel models of Japanese adult males and females of average height and weight, and application of models to radio-frequency electromagnetic-field dosimetry *Phys. Med. Biol.* **49** 1–15

Orcutt N and Gandhi O 1988 A 3-D impedance method to calculate power deposition in biological bodies subjected to time varying magnetic fields *IEEE Trans. Biomed. Eng.* **35** 577–83

Potter M E, Okoniewski M and Stuchly M A 2000 Low frequency finite difference time domain (FDTD) for modeling of induced fields in humans close to line sources *J. Comput. Phys.* **162** 82–103

Wood A W 2008 Extremely low frequency (ELF) electric and magnetic field exposure limits: rationale for basic restrictions used in the development of an Australian standard *Bioelectromagnetics* **29** 414–28